ANALYSIS OF ALTERED VOLCANIC PYROCLASTS USING AVIRIS DATA

William H. Farrand and Robert B. Singer
Planetary Image Research Laboratory, LPL
University of Arizona
Tucson, Arizona

Abstract. Compositional changes that accompany the alteration of volcanic pyroclasts are discernible by visible and near infrared spectrometry. AVIRIS data from the Pavant Butte tuff cone in Millard County, Utah and the Lunar Crater Volcanic Field, Nevada were analyzed in order to map and study the pyroclastic deposits within those areas. Maps of the fractional abundance of select volcanic pyroclasts were produced via spectral mixture analysis. Pyroclastic materials used as spectral endmembers included palagonite tuff, oxidized basaltic cinders and rhyolite. Reference spectra of these and other endmembers were used to calibrate the data to reflectance. Band parameters, extracted from the AVIRIS data, of the 1-μm iron crystal-field absorption in Pavant Butte palagonite tuff indicated the action of spectral mixing between palagonitized and unpalagonitized tuffs. Further analysis of the Pavant Butte data indicated the presence of a previously undetected 2.2 μm Al-OH band in the palagonite tuff.

I. Introduction

Explosive volcanism has played a major role in the Cenozoic history of western North America and many other portions of the world that are adjacent to active plate margins. In many places, the pyroclastic debris from volcanic activity forms the majority of the stratigraphic record for Cenozoic times. Given the importance of such pyroclastic deposits, the ability to map and study them also takes on added significance. Remote sensing systems offer a synoptic view which can be used in an effective manner to analyze the diverse volcanic fields scattered across the globe.

Multispectral systems such as the Landsat Thematic Mapper (TM) have been effectively used in past studies to identify and map volcanic pyroclasts (e.g. Davis et al., 1987). With the advent of imaging spectrometers such as the Airborne Visible/Infrared Imaging Spectrometer (AVIRIS), new possibilities in volcanological research present themselves. While multispectral systems have proven quite effective in mapping volcanic pyroclasts, their limited spectral resolution prevents the unambiguous identification of composition. Imaging spectrometer systems can provide full spectral resolution across all or part of the visible and near infrared wavelength region. The ability to extract near-laboratory quality spectra from remotely sensed data offers the potential to study spatial variations in mineralogy over the extent of volcanic terrains as well to provide clues to the mode of emplacement and environment of alteration of the constituent pyroclastic deposits of such regions.

II. Field Areas

Imagery was acquired over two volcanic terrains within the Great Basin of western North America. The location of the two field areas is shown in Figure 1. The data sets from both regions were collected as part of multi-institution research projects. AVIRIS data were collected over the Pavant Butte tuff cone in Millard County, Utah as part of a Geosat

Committee sponsored research project focusing on the nearby Drum Mountains. AVIRIS and several other advanced airborne scanner data sets were acquired over the Lunar Crater Volcanic Field (LCVF) in northern Nye County, Nevada as part of the NASA-sponsored Geologic Remote Sensing Field Experiment (GRSFE) (Evans and Arvidson, 1991). The AVIRIS data for both Pavant Butte and the LCVF was collected in late September 1989.

Pavant Butte is the most prominent volcanic edifice in the basaltic volcanic fields of the Black Rock Desert of west-central Utah. It was first described by G.K. Gilbert (1890) and more recently by Oviatt and Nash (1989). Pavant Butte lies near the northwestern limb of the Pavant Volcanic Field (Hoover, 1974). The entire region lies in a graben valley within the eastern half of the Great Basin which during the late Wisconsin glaciation was covered by Lake Bonneville. Pavant Butte was erupted into the waters of Lake Bonneville between 16,000 and 15,300 yr B.P. (Oviatt and Nash, 1989).

Pavant Butte closely adheres to the model tuff cone stratigraphy described by Wohletz and Sheridan (1983). The tuff cone consists of a sequence of highly altered palagonite tuffs resting atop flat to shallowly dipping thinly bedded sideromelane (vitric basalt) tuffs. In places the sideromelane tuff is nearly unaltered. The palagonite tuff was originally blanketed by unpalagonitized "mantling tuffs" (Farrand, 1991; Farrand and Singer, in preparation) which have eroded away over broad expanses of the tuff cone to reveal the underlying palagonite tuff.

The second study area is the Lunar Crater Volcanic Field (LCVF) which lies halfway between the towns of Ely and Tonopah in northern Nye County, Nevada. The volcanic field receives its name from Lunar Crater, a spectacular maar crater over 1100 m in diameter and 130 m deep. In addition to Lunar Crater, there is the Easy Chair Crater tuff cone and maar which lies to the north. The LCVF proper consists of over 100 square miles of late Tertiary to Quaternary aged basalt flows, cinder cones and the two aforementioned maar craters (Scott and Trask, 1971).

The basaltic volcanics of the LCVF sit astride a sequence of Tertiary ignimbrites and silicic lava flows. The entire LCVF is, in fact, in the middle of the Lunar Lake caldera, the most recent caldera in the central Nevada caldron complex (Ekren, et al., 1974). The caldera receives its name from the dry lake bed in the middle of the LCVF. The Lunar Lake caldera was formed approximately 25 Ma B.P. About 375 km^3 of ash was ejected to form the tuff currently mapped as the tuff of Lunar Cuesta (Ekren, et al., 1973; Snyder, et al., 1972). The trace of the caldera is preserved today on the east by the arcuate ridge known as "the Wall". Subsequent to the ejection of the tuff of Lunar Cuesta and the accompanying caldera collapse, several more sequences of tuff were erupted interspersed with eruptions of rhyolitic, quartz latitic and andesitic lavas.

III. Volcanic Pyroclasts of Interest

Volcanic tephras can form by magmatic fragmentation, the disruption of magmas by internal volatiles, or by hydromagmatism, the explosive interaction of magma with external water. The nature of the resulting tephras provides clues as to which fragmentation was dominant and, if the latter process was responsible, about the amount of external water present at the time of eruption.

Basaltic hydrovolcanism produces a continuum of volcanic landforms (Wohletz and Sheridan, 1983). While the most prominent examples are the tuff rings and tuff cones produced by Surtseyan activity, even Strombolian edifices such as cinder cones can have phreatomagmatic episodes. Indeed, the oxidized cinders which are common at many cinder cones are probably the result of some small level of water/magma interaction.

Initially basaltic tephras are characterized by a very low overall reflectance. Figure 2a shows reflectance spectra of unoxidized basaltic cinders and nearly pristine sideromelane hydroclasts from Pavant Butte. As basaltic tephras alter, their visual and near infrared reflectance also changes. Figure 2b shows spectra of altered basaltic tephras.

The alteration of cinders takes the form of the development of well crystalline ferric oxide minerals, principally hematite, which have easily recognizable reflectance spectra. The process by which these cinders become oxidized has never been examined in any detail; however, it seems likely that the most oxidized cinders result from relatively high levels of interaction with water, either internal or external to the melt.

A combination of hydration and oxidation of the sideromelane in tuff cones produce the mineraloid palagonite. Palagonite tuffs, such as those from Easy Chair Crater and the cone portion of Pavant Butte, contain zeolites, poorly-crystalline smectite clays and ferric oxides. These components combine to produce reflectance spectra that are brighter and spectrally distinct from the tephras typically found in tuff rings.

With increasing oxidation there is a decrease in the center and depth of the "1-μm" band in laboratory spectra of tuff ring and tuff cone samples (Farrand and Singer, 1991). The laboratory spectra indicate that even as Fe^{3+} becomes more important, i.e. in the palagonite tuff samples, there is no development of a resolvable band at 0.86 or 0.9 μm which could be attributed to well-crystalline hematite or goethite. Instead absorption from ferrous and ferric phases seem to be contributing to one composite feature.

Near infrared spectrometry has also proven very effective in detecting poorly crystalline clay minerals in bulk samples of palagonite tuff. Absorptions at 2.2 μm in several tuff ring samples and at 2.3 μm in many tuff cone samples respectively indicate the presence of Al-OH and Mg-OH bearing clay structures.

In the reflectance spectra of silicic tephras, there is a trend which is in many respects opposite to that seen in the basaltic tephras. While basaltic tephras grow brighter with increasing alteration, silicic tephras grow darker with increasing devitrification (Levine, 1989). Compare the reflectance of the welded tuff in Figure 2a with that of the unwelded tuff in Figure 2b.

IV. Analysis Techniques

The method used to map pyroclastic deposits in this study was a procedure of spectral mixture modelling developed by J.B. Adams, M.O. Smith and co-workers at the University of Washington (e.g., Smith et al., 1990; Gillespie et al., 1990). The spectral mixture analysis used in this study assumes macroscopic mixing and hence is a linear model. The method is based on the assumption that virtually all of the spectral variation within a spectral image can be accounted for by a relatively small number of endmember spectra.

Materials that do not fit into the model reflectance dictated by those endmember spectra contribute to the residuals generated by the method.

There are two types of endmembers. An *image endmember* (*iem*) is the radiance spectrum of one or more pixels that is taken to be representative of a unique type of surface material. A *reference endmember* (*rem*) is a laboratory or field reflectance spectrum of that material. Image endmembers can consist of a mixture of reference endmembers.

The DN of a given band, b (DN_b), can be described in terms of the fractional contributions of its constituent endmembers by the following equation:

$$(1) \qquad DN_b = \Sigma F_i * DN_{i,b} + E_b \text{ with } \Sigma F_i = 1$$

where F_i is the fraction of endmember i; $DN_{i,b}$ is the radiance that endmember i is contributing in band b; E_b is the error for band b; and both summations are carried from i=1 to N where N is the number of endmembers. If there are M bands, the number of endmembers is constrained to be no greater than M + 1. Even for multispectral systems such as the Landsat TM this limit is seldom reached. For a system such as AVIRIS there is actually a surfeit of channels. Since this is the case, it is a good practice to delete the channels with the lowest signal/noise. These bands tend to be those covering the shortest and longest wavelength and those in the middle of atmospheric water absorption features. Consequently the analysis of the LCVF AVIRIS data was done with a 158 channel data set and the analysis of the AVIRIS data for Pavant Butte was done with 150 channels.

Spectral mixture analysis of multi-channel image data generates a fraction image for each endmember. Pixel DN within a fraction image is equivalent to the fractional abundance of that endmember within the area of the pixel. In addition to the fraction images, an RMS error image is generated wherein pixel DN represents the misfit between the image data and the model.

It was noted earlier that image endmembers do not consist of pure materials (although they can be nearly pure). By comparing the image endmember radiance spectra to reflectance spectra of the pure materials that the image endmembers are meant to represent, their actual makeup can be roughly determined. In the process, the image endmembers are "aligned" with their counterpart reference spectra and gain and offset spectra are generated relating image DN to ground reflectance. The equation that describes this process is as follows:

$$(2) \qquad G_b*DN_{i,b} + O_b = \Sigma F_r*R_{r,b} + E_b \text{ with } \Sigma F_r = 1$$

where $DN_{i,b}$ is the radiance or image DN in band b for image endmember i, G_b and O_b are respectively the gain and offset in band b, $R_{r,b}$ is the laboratory or field reflectance in band b for reference endmember r, F_r is the fraction of reference endmember r and E_b is the error in band b.

The values G_b accounts for multiplicative effects such as instrumental gain and atmospheric transmissivity. Likewise, the values O_b account for additive effects such as instrumental dark current and atmospheric path radiance.

V. Results

In the image endmember analysis of the Pavant Butte scene five *iems* were used: shade, playa, palagonite tuff, red soil and vegetation. The LCVF scene was modelled by four *iem*'s: shade, playa, oxidized cinders and rhyolite.

Figure 3 shows fraction images of four of the Pavant Butte *iems* plus the RMS error image. Slide 22 is a color composite of three of these fraction images with palagonite tuff displayed as red, vegetation as green and red soil as blue. The spectral mixture analysis did an excellent job of discriminating the palagonite tuffs. Moreover, the tuff is mapped equally well on both the northern and southern walls of the tuff cone indicating that the inclusion of shade as an endmember has accounted for variable lighting conditions caused by topography.

Slide 23 presents a color composite of the LCVF scene with the cinder fraction image as red, rhyolite as green and RMS error as blue. Vegetation was not included as an endmember thus vegetation-rich areas in the floors of washes appear as blue. Also the northern portion of the Lunar Lake playa appears as blue, indicating that its spectral signature was not modelled well by the playa image endmember (taken from the southern part of the playa). Subsections of the fraction images of cinders and rhyolite are also presented as Figures 4 and 5.

While the cinder fraction image does an excellent job of discriminating oxidized basaltic cinders, the rhyolite fraction image alarms for materials besides rhyolite. The rhyolite is the Rhyolite of Big Sand Spring Valley mapped by Ekren et al. (1974). Alluvial materials also appear bright in Figures 4b and 5b. This is not surprising in light of the fact that such materials are the erosional remnants of the silicic volcanics that surround the LCVF. A close inspection of Slide 22 or Figure 4b also shows some pixels rich in "rhyolite" in the walls of Easy Chair Crater. The reason for this confusion of rhyolite and basaltic tuff becomes apparent in Figure 6 which shows that AVIRIS reflectance spectra of the Rhyolite of Big Sand Springs Valley and Easy Chair Crater palagonite tuff are not dissimilar. Tuff is poorly exposed in the walls of Easy Chair Crater, thus the spectrum in Figure 6 represents a mixture of palagonite tuff and other materials which combine to produce a spectral signature similar to the rhyolite *iem*.

Corresponding laboratory and/or PIDAS spectra were available for all of these endmembers; thus the second stage of reference endmember modelling was conducted. The gains and offsets resulting from this analysis were used to calibrate the data to reflectance. Light and dark target PIDAS and RELAB spectra were also used to calibrate the data to reflectance. Results of the various calibration methods for a 3x3 pixel area of palagonite tuff on the slope of Pavant Butte are shown in Figure 7 with a RELAB sample spectrum (PB-2b) included for comparison. It can be seen in the figure that the empirical line calibration done with PIDAS data resulted in a lower overall reflectance than the empirical line calibration done with RELAB spectra or from the *rem* modelling. Moreover, the scatter in the data points of the two empirical line method calibrations is slightly higher than that which resulted from *rem* modelling. The gains and offsets resulting from the empirical line (RELAB) and *rem* modelling calibrations were each used to convert a portion of the Pavant Butte AVIRIS image cube to reflectance. A 9x9 pixel region on the playa

north of Pavant Butte had a higher standard deviation (over all 150 channels) for the empirical line calibration than for the *rem* modelling method.

This study was part of a larger investigation into the Vis/IR reflectance properties of hydrovolcanic basaltic tephras (Farrand, 1991). As part of the latter study it was discovered that as sideromelane is converted to palagonite, the band parameters of the iron crystal-field band near 1 μm are affected. The palagonitization process converts Fe^{2+} within the sideromelane to Fe^{3+} within poorly crystalline ferric oxides in the palagonite. The result in the 1 μm region is a shortening of that absorption feature's band center and a shallowing of the band depth (Farrand and Singer, 1991). Both of these effects are a consequence of the increasing influence of ferric over ferrous iron phases. The differences in band depth and center as measured at RELAB for samples of sideromelane and palagonite tuff are shown in Figure 8. Included in the sideromelane tuff field are points representing mantling tuff.

The 1-μm feature is clearly detectable on the AVIRIS derived palagonite tuff spectrum shown in Figure 6. 1-μm band parameters for several 3x3 pixel regions of tuff on the flanks of Pavant Butte are also plotted on Figure 8. The fact that the 1-μm band parameters measured by AVIRIS plot between the palagonite and sideromelane tuff fields indicates that there appears to be a mixture of reflected radiance from both palagonitized and unpalagonitized tuffs. This makes sense in view of the physical situation at Pavant Butte where there are broad expanses of palagonite tuff overlain in places by patches of mantling tuff.

Limited field sampling of the Pavant Butte palagonite tuffs missed a mineral phase which was detected by AVIRIS. Spectra of the palagonite tuffs collected (e.g. Figure 3) bore a 2.3 μm Mg-OH vibrational feature, but no 2.2 μm band. However, the 3x3 average pixel spectrum of Pavant Butte palagonite tuff that is shown in Figure 6 indicates that portions of the palagonitized tuff cone do have an absorption at 2.2 μm suggesting the presence of di- as well as trioctahedral clay minerals within the tuff.

VI. Conclusions

Altered volcanic pyroclasts can be readily mapped using a method of spectral mixture modelling. The most discriminable volcanic pyroclasts are those with the most unique spectral signatures. In the Lunar Crater Volcanic Field scene these were the oxidized basaltic cinders. In the Pavant Butte scene it was the palagonite tuff. In the LCVF scene rhyolite was used as an endmember; however, the resulting rhyolite fraction image also alarmed for alluvial materials and the palagonitic tuff of Easy Chair Crater. This non-uniqueness problem might be addressed by making better use of the residual images which can be generated for each band used in the analysis. While the reflectance spectra of Easy Chair Crater tuff and the Big Sand Springs Valley rhyolite resemble each other they are not the same and these differences should show up in the residuals.

Gains and offsets used to calibrate the data to reflectance were generated from both empirical line and reference endmember modelling methods. The latter method was found to be superior in a direct comparison.

Analysis of the Pavant Butte palagonite tuffs in reflectance demonstrated that even with good exposures of a material there can still be contributions to the detected radiance

from other materials within the field of view. In this case, small patches of mantling tuff atop the palagonite tuff skewed the parameters of the 1-μm iron crystal field band from those of pure palagonite tuff to a field between palagonitized and unpalagonitized tuffs. The detection of a previously undetected 2.2 μm absorption in the Pavant Butte palagonite tuffs is a good example of how imaging spectrometry can supplement field observations of altered volcanic tephras.

Acknowledgements

Laboratory sample spectra were obtained at Brown University's RELAB. AVIRIS data of Pavant Butte is courtesy of Bryan Bailey and Jon Dwyer of the U.S.G.S. Sioux Falls. Original code for the spectral mixture modelling work outlined in this paper was provided by John Adams and Milton Smith of the University of Washington. Thanks to Erzsebet Merenyi for help in adapting the spectral mixture code for use at the University of Arizona's Planetary Image Research Laboratory.

References

Davis, P.A., G.L. Berlin and P.S. Chavez, Jr. (1987) Discrimination of altered basaltic rocks in the southwestern United States by analysis of Landsat Thematic Mapper data. *Photogramm. Eng. and Rem. Sens.* **53**, 45-55.

Ekren, E.B., E.N. Hinrichs and G.L. Dixon (1973) Geologic map of The Wall quadrangle, Nye County, Nevada: U.S.G.S. Misc. Geol. Inv. Map I-719, scale 1:48,000.

Ekren, E.B., Quinlivan, W.D., Snyder, R.P., and Kleinhampl, F.J. (1974) Stratigraphy, structure, and geologic history of the Lunar Lake caldera of northern Nye County, Nevada. Jour. Res. U.S.G.S., 2, 599-608.

Evans, D.L. and R.E. Arvidson (1991) An overview of the Geologic Remote Sensing Field Experiment (GRSFE). *EOS (Trans. Am. Geophys. Union)* **72** (Spring meeting supplement), 176.

Farrand, W.H. (1991) Visible and near infrared reflectance of tuff rings and tuff cones. Ph.D. dissertation, University of Arizona, Tucson, 187 pp.

Farrand, W.H. and R.B. Singer (1991) Oxidation of basaltic tephras: Influence on reflectance in the 1 μm region. *Lunar and Planetary Science XXII*, Lunar and Planetary Institute, Houston, 365-366.

Farrand, W.H. and R.B. Singer, Alteration of hydrovolcanic basaltic ash: Observations with Vis/IR spectrometry. (paper in preparation for *J. of Geophys. Res.*)

Gilbert, G.K. (1890) Lake Bonneville: *U.S. Geological Survey Monograph 1*, 438 pp.

Gillespie, A.R., M.O. Smith, J.B. Adams, S.C. Willis, A.F. Fischer III and D.E. Sabol (1990) Interpretation of residual images: Spectral mixture analysis of AVIRIS images, Owens Valley, California. *Proceedings of the Second Airborne Visible/Infrared Imaging Spectrometer (AVIRIS) Workshop.* R.O. Green (ed.) JPL Publication 90-54, Jet Propulsion Laboratory, Pasadena, CA, 243-270.

Hoover, J.D. (1974) Periodic Quaternary volcanism in the Black Rock Desert, Utah. *Brigham Young University Geology Studies* **21**, 3-72.

Levine, A. (1989) Ash-flow zones of the Bishop Tuff: Detailed mapping with the Landsat Thematic Mapper. M.S. thesis, Arizona State University.

Oviatt, C.G. and W.P. Nash (1989) Late Pleistocene basaltic ash and volcanic eruptions in the Bonneville basin, Utah. *Geol. Soc. America Bull.* **101**, 292-303.

Scott, D.H. and Trask, N.J. (1971) Geology of the Lunar Crater volcanic field, Nye County, Nevada. USGS Prof. Paper 599-I.

Smith, M.O., S.L. Ustin, J.B. Adams and A.R. Gillespie (1990) Vegetation in deserts: 1. A regional measure of abundance from multispectral images. *Rem. Sens. Env.* **31**, 1-26.

Snyder, R.P., E.B. Ekren and G.L. Dixon (1972) Geologic map of the Lunar Crater quadrangle, Nye County, Nevada. U.S.G.S. Misc. Geol. Inv. Map I-700, scale 1:48,000.

Wohletz, K.H. and M.F. Sheridan (1983) Hydrovolcanic explosions II: Evolution of basaltic tuff rings and tuff cones. *Am. J. Sci.*, **283**, 385-413.

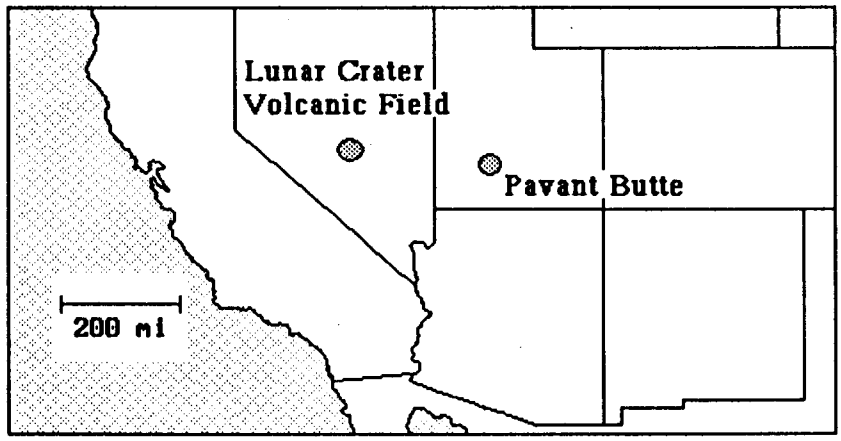

Figure 1: Locations of field sites.

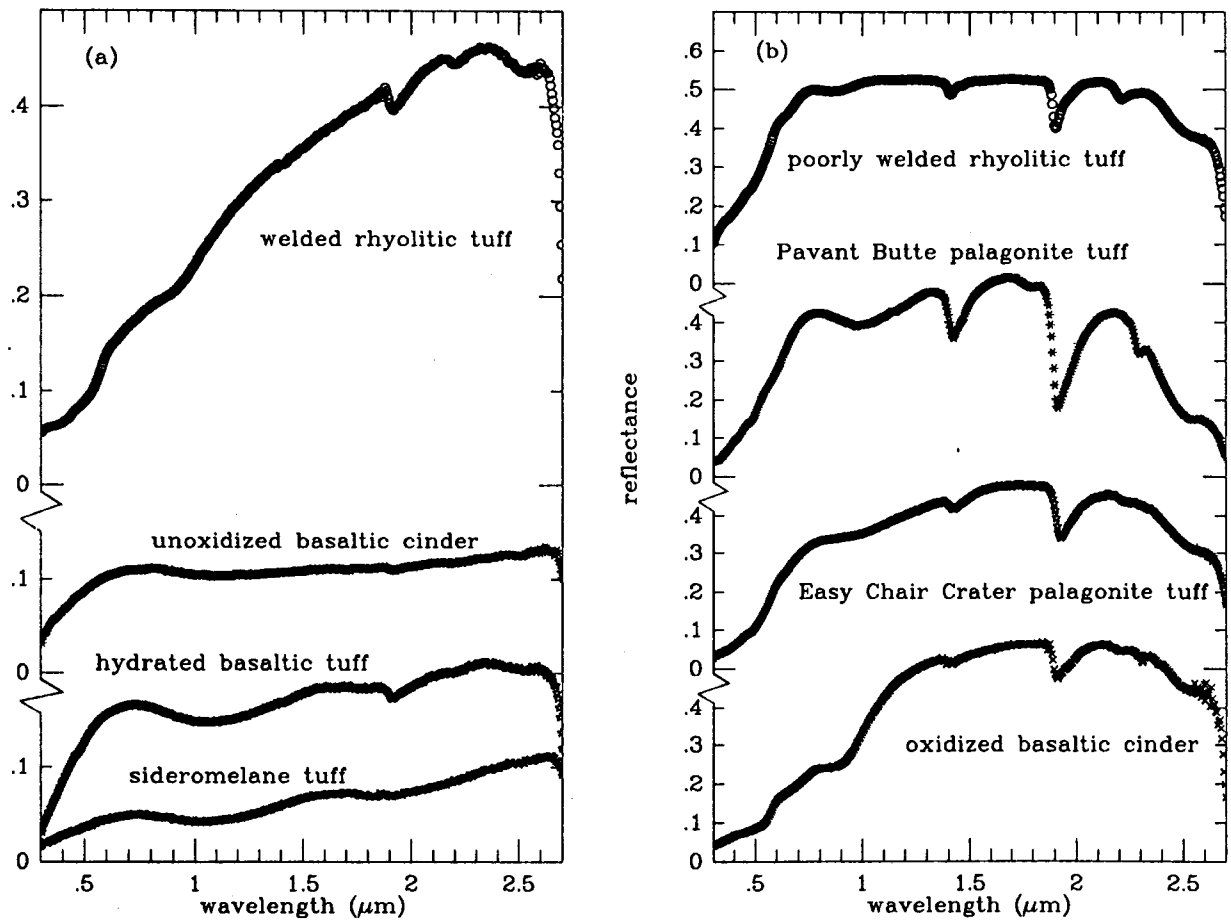

Figure 2: Reflectance spectra of volcanic pyroclasts measured at RELAB.

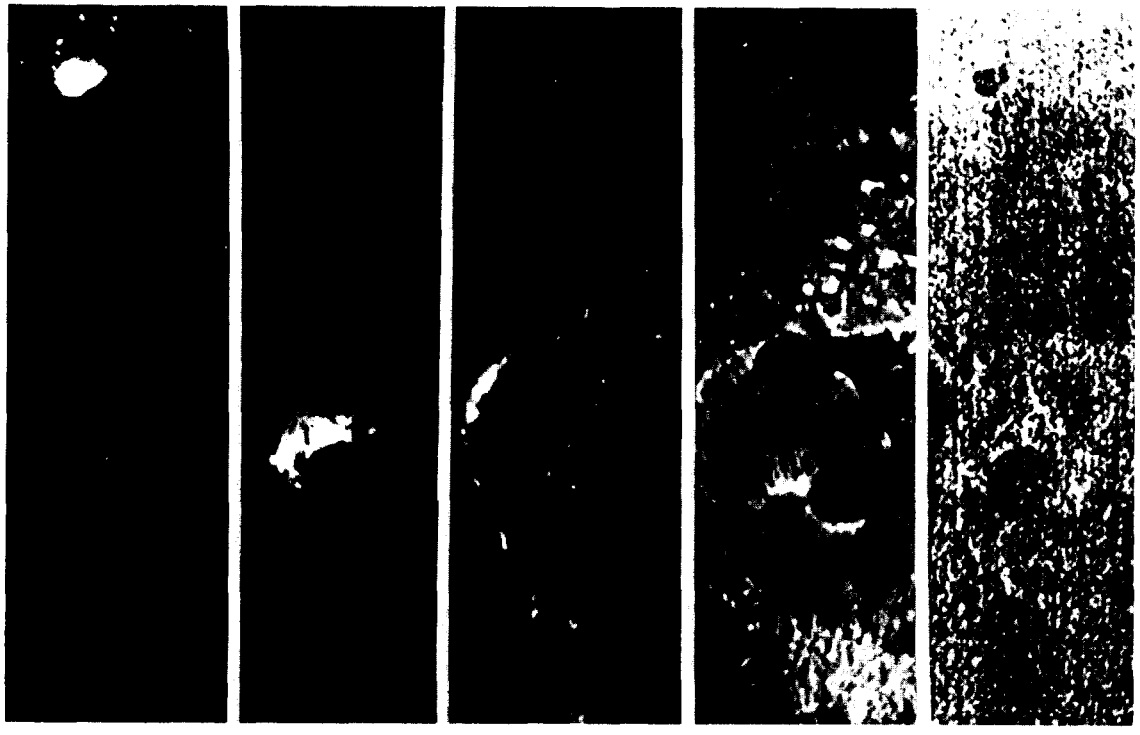

Figure 3: Fraction images of Pavant Butte *iems* plus RMS error. From left to right: playa, palagonite tuff, vegetation, red soil and RMS error. Shade is not shown.

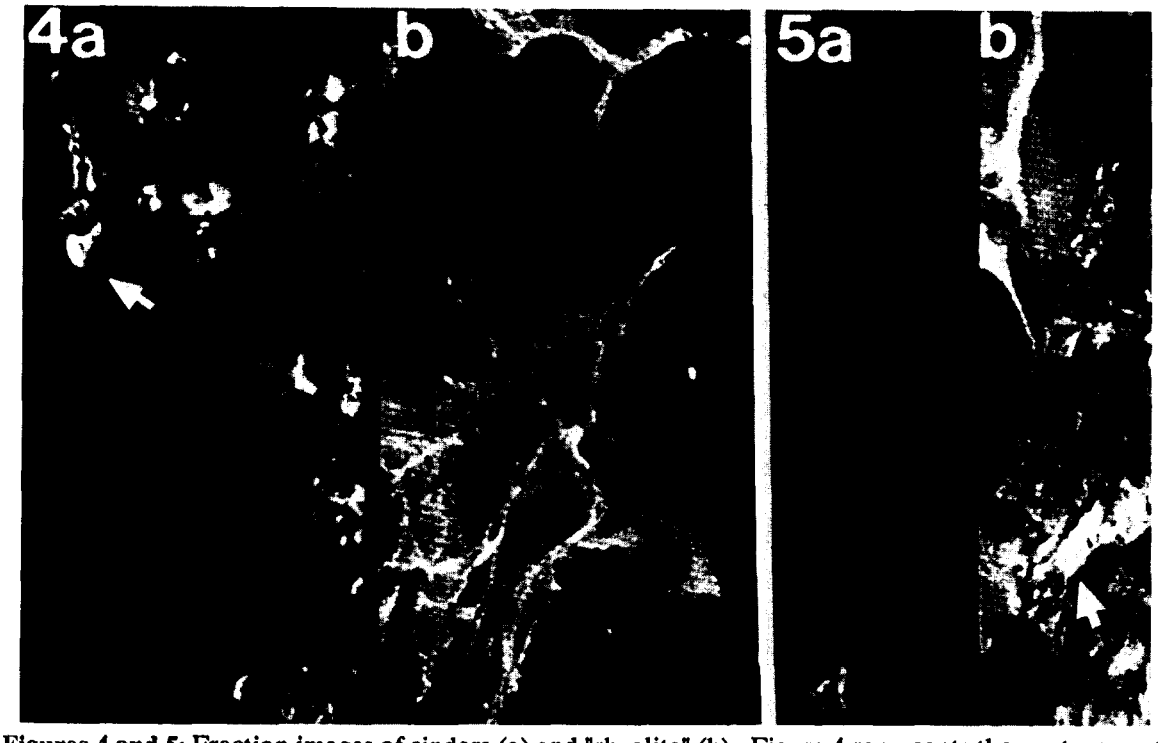

Figures 4 and 5: Fraction images of cinders (a) and "rhyolite" (b). Figure 4 represents the western portion of the LCVF scene. The cinder *iem* was extracted from the cinder cone north of Easy Chair Crater (indicated by the arrow). Figure 5 is the eastern portion of the LCVF scene. The arrow indicates where the rhyolite *iem* was extracted from.

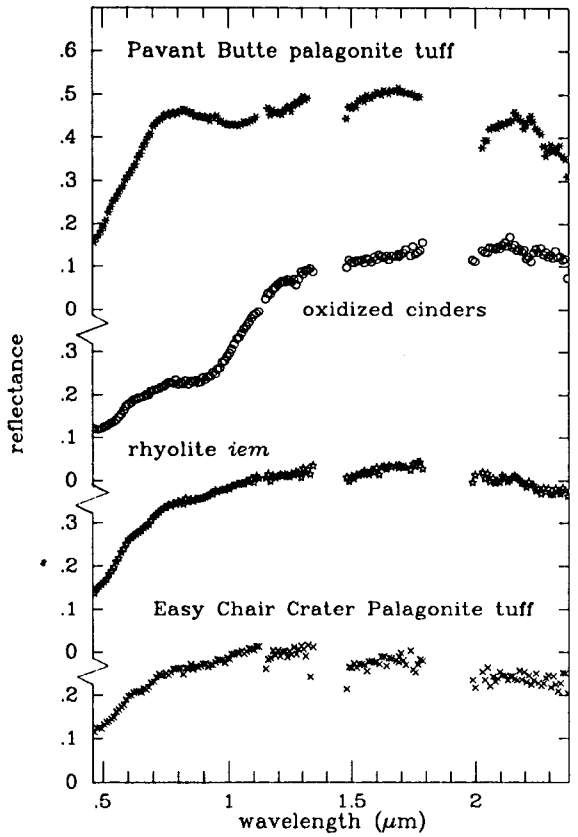

Figure 6: Reflectance spectra of volcanic pyroclasts extracted from AVIRIS image data. The resemblance of Easy Chair Crater tuff and the rhyolite *iem* accounts for basaltic tuff alarming as rhyolite in Figure 4a.

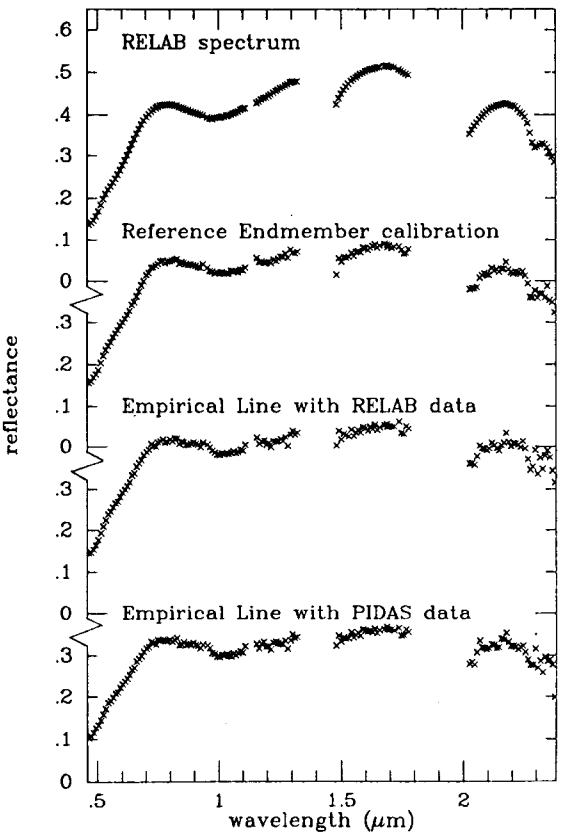

Figure 7: Comparison of methods for calibration to reflectance.

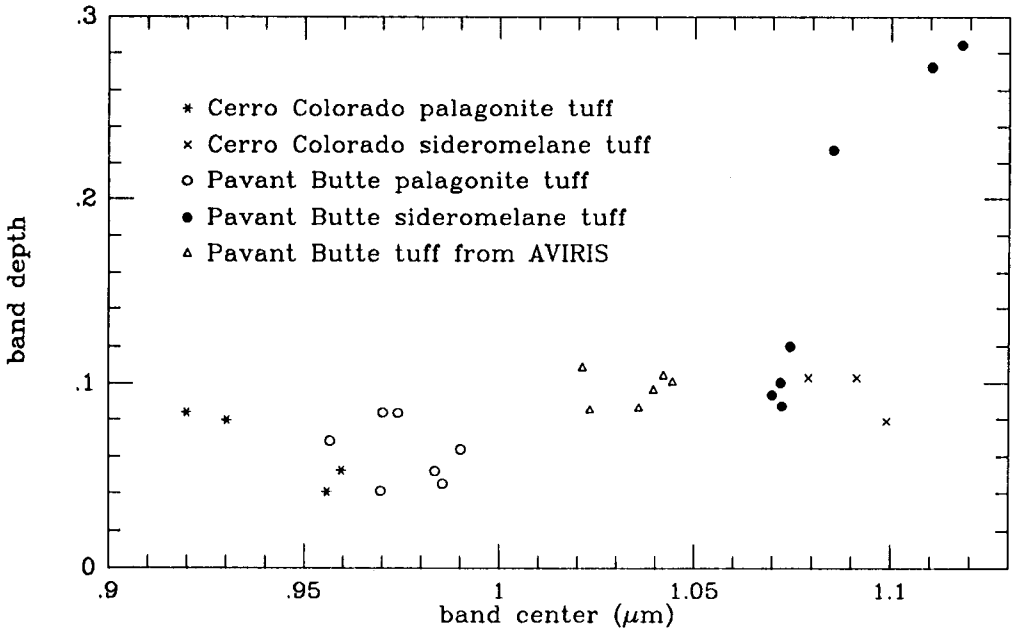

Figure 8: Band Depth vs. Band Center of 1 - μ feature